The Influence of Flow Field Design on Zinc Deposition and Performance in a Zinc-iodide Flow Battery

Journal:	*ACS Applied Materials & Interfaces*
Manuscript ID	am-2021-09770x.R1
Manuscript Type:	Article
Date Submitted by the Author:	n/a
Complete List of Authors:	ShakeriHosseinabad, Fatemeh; University of Calgary, Chemical and Petroleum Engineering Randjbar Daemi, Sohrab; University College London, Chemical Engineering Momodu, Damilola; University of Calgary, Department of Chemical and Petroleum Engineering Brett, Dan; University College London, Chemical Engineering Shearing, Paul; University College London, Chemical Engineering Roberts, Edward; University of Calgary, Department of Chemical and Petroleum Engineering

The Influence of Flow Field Design on Zinc Deposition and Performance in a Zinc-iodide Flow Battery

Fatemeh ShakeriHosseinabad,[†] Sohrab R. Daemi,[‡] Damilola Momodu,[†] Dan J.L. Brett,[‡] Paul R. Shearing,[‡] and Edward P.L. Roberts*[,†,‡,¶]

†*Department of Chemical and Petroleum Engineering, University of Calgary, 2500 University Drive NW, Calgary, Alberta, Canada T2N 1N4*

‡*Electrochemical Innovation Lab, Department of Chemical Engineering, University College London, London WC1E 7JE, United Kingdom*

¶*ORCID(s): 0000-0003-2634-0647*

**Corresponding author: Edward.P.L Roberts*

E-mail: Edward.Roberts@ucalgary.ca

Phone: +1 4032204466

Abstract

Among the aqueous redox flow battery systems, redox chemistries using a zinc negative electrode have a relatively high energy density, but the potential of achieving high power density and long cycle life is hindered by dendrite growth at the anode. In this study, a new cell design with a narrow gap between electrode and membrane was applied in a zinc-iodide flow battery. In this design, some of the electrolyte flows over the electrode surface, and a fraction of the flow passes through the porous felt electrode in the direction of current flow. The flow battery was tested under constant

current density over 40 cycles and the efficiency, discharge energy density and power density of the battery were significantly improved compared to conventional flow field designs. The power density obtained in this study is one of the highest power densities reported for the zinc-iodide battery. The morphology of the zinc deposition was studied using scanning electron microscopy and optical profilometry. It was found that the flow through the electrode led to a thinner zinc deposit with lower roughness on the surface of the electrode, in comparison to the case where there was no flow through the electrode. In addition, inhibition of dendrite formation enabled operation at a higher range of current density. Ex-situ tomographic measurements were used to image the zinc deposited on the surface and inside the porous felt. Volume rendering of graphite felt from X-ray computed tomography images showed that in the presence of flow through the electrode, more zinc deposition occurred inside the porous felt, resulting in a compact and thinner surface deposit, which may enable higher battery capacity and improved performance.

Key words: Zinc-iodide, Zinc deposition, Flow field design, Flow-by-through, Battery performance, X-ray computed tomography

Introduction

Redox flow batteries (RFBs) technologies are considered a promising candidate for medium and large-scale energy storage systems.[1,2] Unlike conventional batteries, energy and power generation can be independently scaled in RFBs.[3,4] Several types of flow battery systems such as vanadium and zinc-based RFBs have been reported and commercialized.[5,6]

Due to their high reversibility and power output, the vanadium redox flow battery is the most developed; however, the electrolyte for this system has a high cost. In order to reduce the cost, active materials such as zinc compounds can be used.[7–9] Zinc-based flow batteries are attractive because they have high aqueous solubility and hence high energy density, as

well as rapid kinetics.[4,5] Unlike other secondary batteries based on metals (eg, Li, and Na), zinc-based batteries are stable in air, and non-flammable.[7,10] Among the aqueous redox flow batteries, the zinc-iodide flow battery has been reported to have very high discharge energy density.[7] However, aqueous zinc batteries suffer from dendrite formation resulting in capacity fading and a decreased battery performance. In addition, dendrites can grow through the membrane causing short circuiting and failure of the battery. They can also fracture causing capacity fading as the dissolved zinc ion concentration decreases.[11,12]

A cyclable uniform zinc deposition at high current density is necessary for commercialization of secondary zinc-based batteries.[13,14]

The equilibrium shape of crystals is controlled by surface energy, γ, which is the interfacial excess free energy per unit area of a particle crystal facet.[15] Anisotropy in solid-liquid interfacial energy plays a critical role in dendrite growth and the crystallographic growth direction of dendrites.[16] It has been reported that the presence of surface energy anisotropy changes morphology in the interfacial dynamics leading to dendritic growth with regular structure.[17,18] Wang et al. found that at high current density a formation of a leaf-like morphology was obtained which may be due to powerful surface energy anisotropy.[19] Recently a new zinc-based system was reported where dendrite formation could be controlled in a multiphase electrolyte by rational design of electrodeposition conditions.[20] Dendrite formation does not develop until the overpotential reaches a critical value.[21] Local current density, concentration and temperature are important factors in the time required to form dendrites.[21,22] At high cell voltage, experienced during charging, the electrochemical reaction at the negative (zinc) electrode is driven into a mass transport controlled regime and dendrite growth occurs at a faster rate.[21,23] An inhomogeneous electric field and large ionic concentration gradients (associated with mass transport control) have been reported to be the main causes of dendrite formation.[24,25] Increasing the flow rate increases the rate of mass transport; hence, increasing mass transport suppresses local zones of high current densities, and decreases zinc ion concentration gradients. This leads to the participation of more

ions in electrochemical reactions and a more uniform zinc deposition onto the electrode surface.[19] Thus, the crystallinity and characteristics of the zinc deposit depend upon the mass transport conditions and the current density distribution during charging.[26,27] Dendrite and layer-like zinc deposit have been reported for high (30 mA cm^{-2}) and medium (20 mA cm^{-2}) current density respectively.[26] Based on the crystallinity of the zinc deposition, dendritic deposits formed at high current density have a tree-like (dendritic) morphology, while deposits formed at slower rates of deposition have a hexagonal shape.[26] Low overpotential (50 mV) resulted in a layer-like growth of zinc deposition, and higher overpotential (100 mV) resulted in nucleation and uniform growth of boulder deposits.[28] However, factors that control the initiation of dendrite formation are not independent. A universal overpotential, current density, and electrolyte flow rate to prevent dendrite deposition has not been reported.[26]

Higher zinc concentration, elevated temperature of the electrolyte and high electrolyte flow rate suppress dendrite formation.[29,30] The hydrodynamics of electrolyte and the battery configuration affect the zinc deposit morphology and dendrite growth direction,[10,30,31] dendrite formation is mainly controlled by diffusion limitations.[11,26,29–32]

Flow field design plays a key role in the performance and power density of the redox flow battery systems.[33] In a zinc-bromine battery system with a "flow-by" (FB) flow field (i.e. with the electrolyte flowing across the electrode surface, in the gap between the electrode and membrane), much smaller/smoother surface features have been observed in the zinc deposit in comparison with non-flow electrolyte systems.[13] Parametric studies of zinc deposition on a porous carbon substrate in the same system showed that with increasing Reynolds number (up to 500) or current density, the extent of the zinc deposition within the porous electrode increased.[13]

The effect of deposition conditions on the morphology of zinc deposition in alkaline media has also been evaluated by scanning electron microscopy (SEM).[26,28] The dendrite growth and its volume-specific loading in rechargeable zinc-based was recently examined using X-ray computed tomography (X-ray CT) to study the battery failure mechanism due to dendrite

formation.[21,34]

An aqueous zinc-iodide RFB with a high energy density has been reported.[7] Zinc-iodide has a very high solubility in water with a relatively high thermodynamic open-circuit potential of 1.30 V. The main redox reactions in the zinc-iodide RFBs are shown in equations (1) and (2) for the positive and negative side of the battery respectively.[35]

$$\text{Cathode} : I_3^- + 2e^- \leftrightarrow 3I^- \quad E^0 = 0.536V \quad \text{vs} \quad \text{SHE} \tag{1}$$

$$\text{Anode} : Zn \leftrightarrow Zn^{2+} + 2e^- \quad E^0 = -0.763V \quad \text{vs} \quad \text{SHE} \tag{2}$$

The influence of flow field design on the morphology of zinc deposition and electrochemical performance of the zinc-iodide system was investigated. The electrolyte was studied by Raman spectroscopy to evaluate the battery system reversibility. The deposit morphology was studied using SEM, optical profilometry and micro X-ray CT to evaluate the influence of flow field design on the zinc deposition morphology. In addition, the particle size, roughness of the electrode surface and depth of zinc penetration inside the porous carbon substrate were explored. Optical profilometry and X-ray CT was used to measure the zinc deposition quantitatively and qualitatively. A new flow arrangement was used which has not previously been studied in zinc RFBs, where part (or all) of the flow goes through the electrode to enhance the mass transfer rate. By enhancing the mass transport rate, this flow arrangement can enhance the battery power density and cycling stability. A comprehensive study of the zinc deposit morphology provides insight into the impact of the flow arrangement on the zinc electrode during battery cycling. Due to dynamic structural change during metal plating and stripping, the design of the flow field in hybrid flow batteries is more complicated than for all liquid systems. The influence of flow field design on the performance of hybrid flow

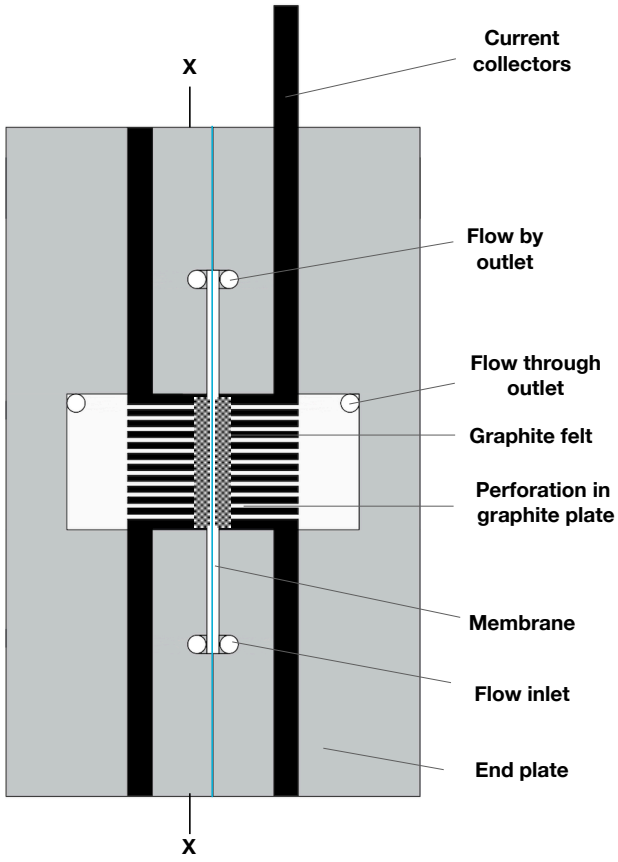

Figure 1: Schematic illustration of the design of the zinc-iodide RFB test cell, showing cross-sections through the cell. Different electrolyte flow modes were applied, using valves on the outlet ports, including FB, where the electrolyte flowed across the surface of each electrode, 'flow-through', where all the electrolyte flowed through electrode on each side of the cell and FBT mode, where some of the electrolyte flowed through the electrode on each side of the cell. Electrolyte flowing through the electrode exited via a compartment behind the perforated graphite plate current collector.

batteries has rarely been investigated.[36] Recently a Sn-Fe flow battery with relatively stable performance over 700 cycles was reported.[37] The impact of serpentine and interdigitated flow field designs on Sn-Fe flow battery performance has also been investigated.[36] It was found that the design of the flow field is critical to avoiding blockage of mass/ion transport pathway and achieve a uniform product distribution in hybrid flow batteries.

The experimental operating conditions aimed to evaluate the battery performance for three different flow field conditions under the same operating conditions and electrode ma-

terials. Zinc deposition in the FB flow field design is associated with a relatively low rate of mass transport to the electrode surface. In this study, a new flow arrangement is considered by adding a flow-through component to the flow field in both the positive and negative side of the battery. The combination of FB and flow-through (here called FBT) enables an enhanced rate of mass transport rate by adding a velocity component towards the electrode, and increased utilization of the internal surface area of the electrodes. In addition, only a part of the flow was directed through the electrodes, so that the pressure drop remains relatively low. It was expected that this flow arrangement would increase the uniformity of the current distribution, achieve a more compact and uniform zinc-deposit, suppress dendrite formation and enhance performance by reducing mass transport overpotential and increasing active area. In addition increased zinc-deposition within the electrode could enable operation with higher capacity per unit area with a thinner deposit on the electrode surface.

Experimental details

Zinc-polyiodide flow cell

Zinc-iodide (Sigma-Aldrich, 99 wt.%) dissolved in deionized water (18.2 M Ωcm resistivity) was used to prepare the electrolyte system on the positive and negative side. The cell design is illustrated in Figure 1 by a cross-section through the cell. In addition, cross-section X-X (location indicated in Figure 1) and the photographs of a zinc-iodide single cell are shown in Figure S1. The detailed design of the perforated graphite plate is shown in Figure S2. In each half-cell, a 5 cm^2, 2 mm thick graphite felt (Fuel Cell Store, US, CT GF020) was used as the electrode and a perforated graphite plate as the current collector. A peristaltic pump (Cole-Parmer, Masterflex Model 07551-30) with high-pressure Neoprene tubing (4.8 mm inner diameter, Masterflex Norprene, Cole-Parmer) and two glass reservoirs of electrolyte were connected to the flow cell during the evaluation of battery performance. A volume of 20 mL of electrolyte was pumped to the positive and negative half-cells at a flow rate of 20

ml min^{-1}. The two operating modes, FB, flow through and FBT were obtained by closing respective valves on the outlet of the cell.

In the flow-through operating mode, valves at the exit at the top of the cell (between the electrodes) were closed and the electrolyte was forced to flow through the electrodes, exiting via a compartment behind the graphite plate. In the FB operating mode, valves at the exit at the top of the cell (between the electrodes) were opened and valves at the exit from the compartment behind the graphite current plate were closed and electrolyte was forced through the valves at the top of the cell. In the FBT mode, all valves were opened so that the electrolyte flow was split between both routes, some flowing through and some between the electrodes and membrane. The electrode compartments were separated by a cation exchange Nafion membrane (DuPont, NF 117/H^+), and the cell was sealed using polyvinyl chloride (PVC) gaskets (Mcmaster-Carr, US) compressed by PVDF end-plates. The gap between each electrode surface and the membrane was 2 mm. The current density for the long-term charge/discharge characteristics of the zinc-iodide battery in this study is 20 mA cm^{-2}. A fixed time was used for charging; however, if the cell voltage reached a cut-off of 1.5 V (at a current density of 20 mA cm^{-2}) the charging was terminated early to protect the electrodes. Discharging was carried out to a lower cut-off cell voltage of 0.5 V.[2,38] The galvanostatic charge/discharge characteristics and electrochemical impedance spectroscopy (EIS) was performed using a potentiostat (Metrohm Autolab PGSTAT 320N).

Characterization of zinc deposit

The morphology of zinc deposition on the battery electrodes was characterized by SEM. The SEM used was a quanta FEG 250 FESEM (Thermo Fisher Scientific). It is equipped with Bruker Esprit X-ray micro-analysistem consisting of a Quantax 5030 energy dispersive X-ray spectrometer, Bruker SVE signal processing unit, and Esprit version 2.2 software. All imaging and analysis was performed under high-vacuum conditions with an accelerating potential ranging from 5 kV to 15 kV.

A non-contact optical profilometry technique was used with a Zescope optical profilometer controlled by a Zemetrics Zemaps software (version 1.16.78) to compare the morphology of the zinc-electrodeposition in the different flow modes and characterize the topography of the zinc deposition.

A square-shaped sample of ca. 5 mm × 5 mm was cut from the center of each felt for X-ray CT analysis and stacked on an SEM stub using Kapton tape to separate each layer from the one below. X-ray CT imaging was carried out using a Zeiss Xradia Versa 520, with a 60 kV tube voltage and magnifications of 4 and 20 X with exposure times of 15 and 30 s respectively. No pixel binning was applied resulting in a pixel size of ca. 1.8 and 0.4 µm for the 4 and 20 X scans respectively. The radiographs were reconstructed using a commercial filtered-back-projection algorithm[39] into 3D volumes. This is implemented in the XMReconstructor software by Carl Zeiss Inc. Image visualization, data segmentation and analysis were carried out in Thermo Fisher Scientific's Avizo software and ImageJ. The 20 X scans were segmented with the aid of thresholding tools. The volume renderings were generated in Avizo from the 2D label fields. The 20 X scans were segmented with the aid of thresholding tools. The contrast differences between pore, carbon and zinc were used to assign each pixel to its respective phase. Due to the high attenuation of zinc, it appeared as bright spots throughout the images, whereas the carbon felts were identified due to their elongated shapes and darker contours.

Table 1: **Zinc-iodide battery charge/discharge performance as a function of current density for FB and FBT operating modes.**

Current density mA cm^{-2}	**FB[a] QE[b]** (%)	**FB VE[c]** (%)	**FB EE[d]** (%)	**FBT[e] QE** (%)	**FBT VE** (%)	**FBT EE** (%)
10	96.5	83.3	80.3	99.5	90.8	90.3
20	96	72	69.1	99	85.8	84.9
30	95.5	67	63.9	97.8	76	74.3
70	76	50.6	38.5	88	55	48.4

[a]FB: flow-by; [b]QE: coulombic efficiency; [c]VE: voltage efficiency
[d]EE: coulombic efficiency; [e]FBT: flow-by-through

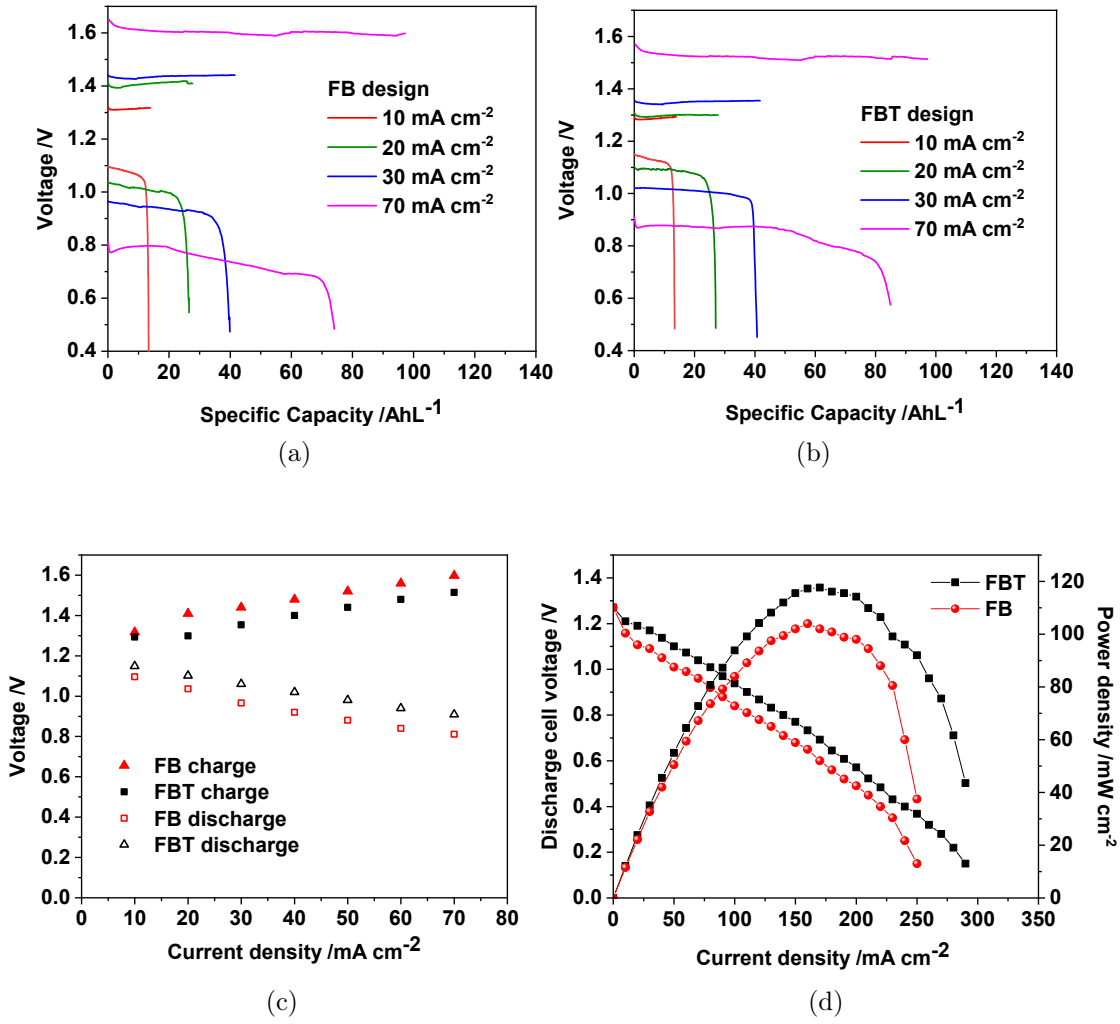

Figure 2: Galvanostatic voltage profile curves of a 5 cm^2 flow battery using a 3 M ZnI_2 electrolyte (20 mL on each side) under constant current densities in a range of 10, 20, 30, and 70 mA cm^{-2}, at **(a)** FB, and **(b)** FBT mode, and **(c)** variation of the cell voltage at the end of charging and the initial discharge with current density. **(d)** Discharge polarization curves and corresponding power density curves of a 3 M ZnI_2 flow battery at 80% State-of-charge with Nafion 117.

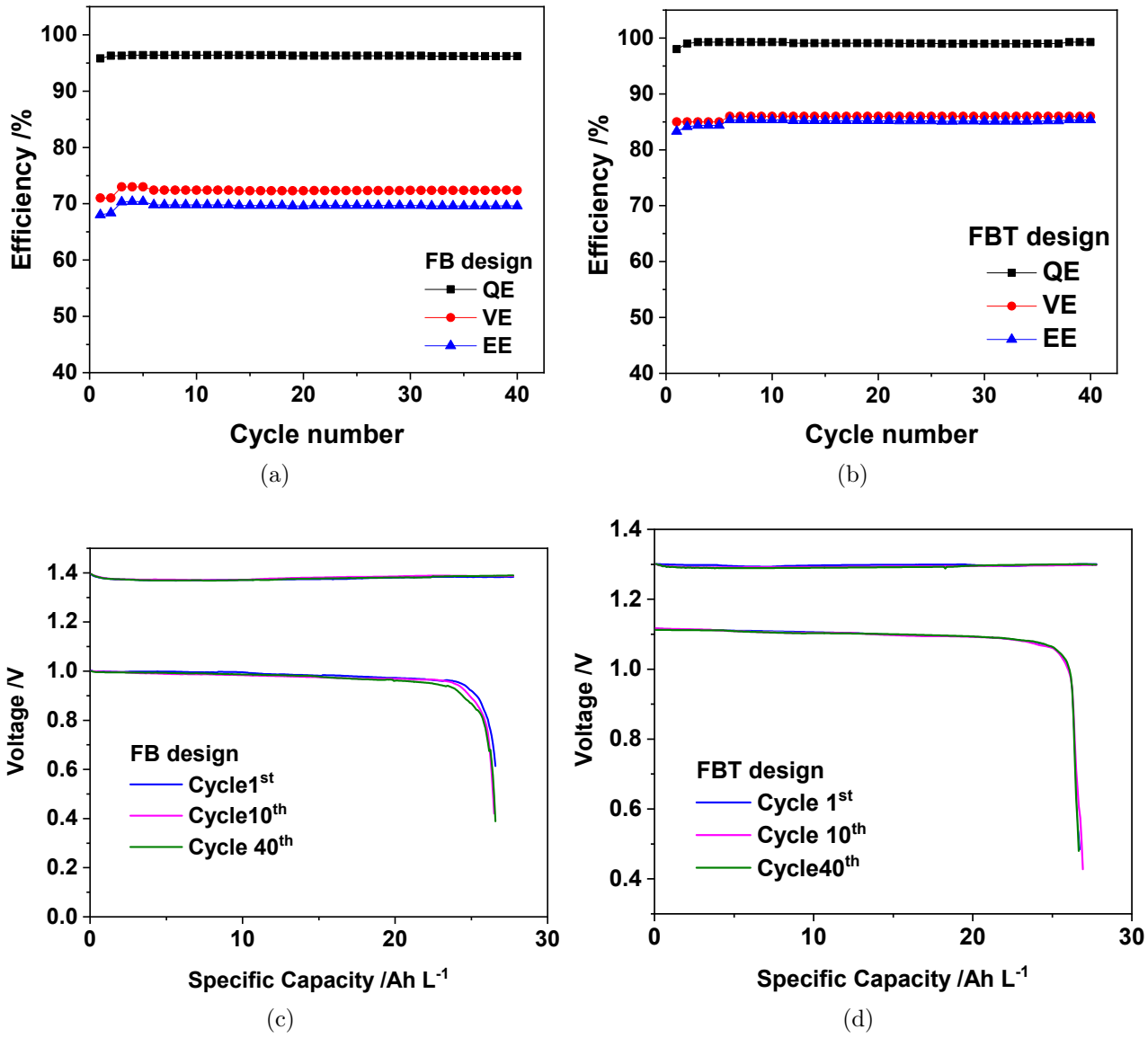

Figure 3: **(a)** Efficiencies during 40 cycles of charge/discharge for ZnI_2 RFB with 3 M ZnI_2 (20 mL on each side), Nafion 117 membrane, operating at a current density of 20 mA cm^{-2} with a charge duration of 20,000 s, corresponding to state-of-charge of 25.7% in **(a)** the FB and, **(b)** the FBT mode. **(c)** Galvanostatic voltage profile for three different cycles of zinc-iodide battery shown in **(a)**. **(d)** Galvanostatic voltage profile for three different cycles of zinc-iodide battery shown in **(b)**.

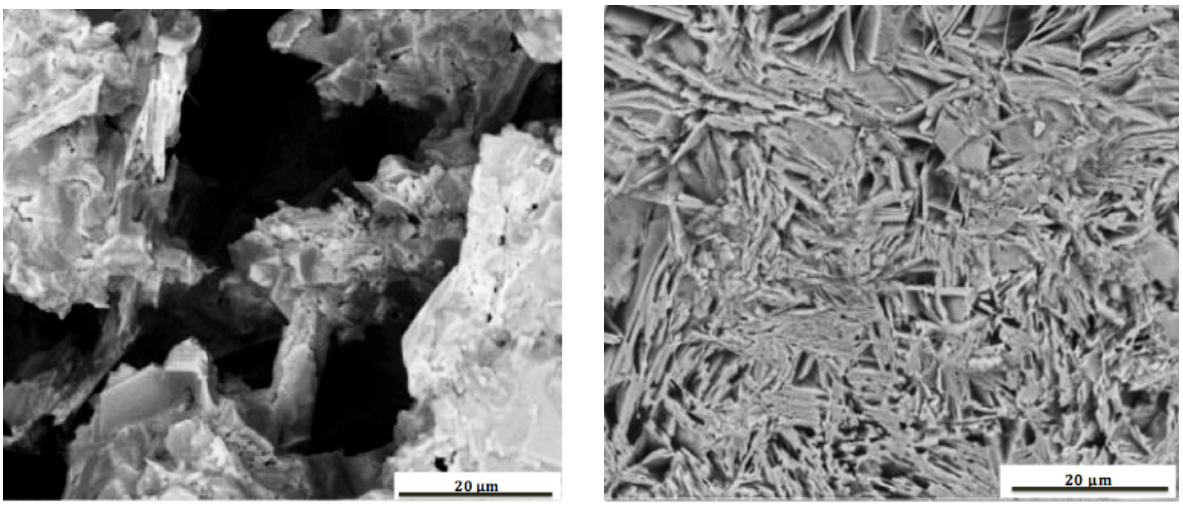

(a) (b)

Figure 4: SEM images of the surface [**(a)** and **(b)**] of the zinc electrode in the ZnI_2 RFB after charging with an 3 M ZnI_2 electrolyte at a current density of 20 mA cm^{-2}, zinc deposition formed after charging in cycle 40th. The battery was operated in **(a)** FB and **(b)** FBT.

Results and discussions

The influence of flow mode on the Zn-I flow battery performance

In both flow modes, the potential losses observed during charge/discharge cycles increased with current density, as expected. At high current density (i.e. ≥ 30 mA cm^{-2}), the increased overpotential and surface energy anisotropy is expected to result in mass transport limitation and dendrite formation.[19] The coulombic efficiency (QE), voltage efficiency (VE) and energy efficiency (EE) of the battery at different current densities are shown in Table 1. In the FBT mode, significantly lower potential losses (and hence higher VE and EE) were observed, particularly at the highest current density studied of 70 mA cm^{-2}. At this current density, in the FBT mode, the coulombic efficiency was 88 % and the discharge capacity was 88 Ah L^{-1}, significantly higher than the values of 76% and 72 Ah L^{-1} obtained in FB mode.

The improvement in performance obtained in FBT mode is likely due to a reduction in the contact resistance, and enhancements in the mass transport rate at both electrodes. The reduction in contact resistance was confirmed by EIS (Figure S3), which showed a 17% lower ohmic resistance for the FBT mode compared to FB. The lower ohmic resistance may be due

to the pressure difference caused by the flow through the felt electrode towards the current feeder, leading to lower contact resistance. No zinc deposition was observed on the surface or in the perforations of the graphite plate, confirming that it was acting as a current feeder and did not participate in the electrochemical reactions.

The increased mass transfer rate is expected to lead to a smaller overpotential on both sides of the battery and a smoother zinc deposit on the negative electrode.[19] As shown in Figure 2 (a) and (b), in the FBT mode, a lower overpotential and potential loss was observed at all current densities studied, due to enhanced mass transport. The cell voltage at the end of charging and initial discharge potential for current densities from 10 to 70 mA cm^{-2} are shown in Figure 2 (c). In the FBT design, the convection of electrolyte flowing through the porous electrode enhances the mass transport rate and effective surface area, decreasing the overpotential in all cases, leading to improved performance. The enhanced mass transport obtained in FBT mode can be expected to suppress dendrite formation. A low charge efficiency (below 90%) was observed at the highest current density of 70 mA cm^{-2} in both FB and FBT mode this is likely due to mass transport limitations on the iodine side of the battery, or zinc dendrite detaching from the negative electrode. The higher cell voltage during charge, could lead to larger overpotentials, dendritic deposition and side reactions. Similarly, low charge efficiency has been reported for a current density of 80 mA cm^{-2} for the zinc-cerium battery.[38] In hybrid flow batteries, a reduction in charge efficiency may be due to crossover, or shedding of dendritic deposits at the negative electrode. Dendrite formation decreases the utilization of zinc deposited on the electrode during the discharging process, and hence decreases the charge efficiency.[21,40,41] Increasing mass transfer at the membrane can lead to increased transport of oxidized species from the positive electrolyte, decreasing the charge efficiency. The addition of a flow component through the felt electrode towards the current feeder in the FBT mode is expected to enhance the mass transfer rate in the porous electrode, however it will also lead to a reduction in the flow velocity across the membrane surface, which may reduce the rate of crossover. In addition, inhibition of dendrite formation

and formation of a compact and uniform zinc deposition resulted in improvement coulombic efficiency, cycle life and performance of the battery. This is a consequence of more complete dissolution of the zinc deposit, maintaining the zinc concentration at a stable level.[21,40,41] Polarization studies of the zinc-iodide battery were performed at 80% state-of-charge, as shown in Figure 2 (d). The battery was able to deliver a maximum power output of 118 mW cm^{-2} and 104 mW cm^{-2} in the FBT and FB designs respectively. The power density of 118 mW cm^{-2} obtained at 80% SOC is amongst the highest reported for a flow battery using a ZnI_2 electrolyte. Power densities reported for flow batteries using a pure zinc iodide electrolyte have ranged from 50 mW cm^{-2},[42] to 150 mW cm^{-2}.[43] Note that these previous studies were obtained at 100% SOC compared to only 80% used in this study. As well as the high power density for a pure ZnI_2 electrolyte, Jian et al.[43] were able to achieve a power density of 310 mW cm^{-2} in a zinc iodide flow battery by adding an NH_4Br supporting electrolyte, which could also be applied with the FBT design. The performance of the Zn-I battery, as well as the morphology of the zinc deposit were investigated in the two different flow arrangements: FB and FBT. The variation of the coulombic efficiency, voltage efficiency, and energy efficiency for 40 cycles of charge/discharge of a Zn-I battery using 3.0 M ZnI_2 electrolyte at 20 mA cm^{-2} is shown in Figure 3 (a) and (b). In the FBT design, a significant improvement in the performance was obtained. In the FB mode as shown in Figure 3 (c), the cell voltages at the end-of-charge and beginning-of-discharge were 1.40 V and 1.001 V respectively, indicating a potential loss of ca. 400 mV. A stable coulombic efficiency of 96 % , voltage efficiency of 72 % and energy efficiency of 69 % were obtained with the FB operation at 20 mA cm^{-2}. In the FBT design shown in Figure 3 (d), the cell voltages at the end-of-charge and beginning-of-discharge were 1.31 V and 1.11 V; indicating potential losses of approximately 200 mV. The average coulombic efficiency, voltage efficiency and energy efficiency were significantly higher for the FBT operating mode, at 99%, 85.8%, and 85% respectively. During the discharge phase in the FBT design, the discharge capacity was slightly higher than that in the FB mode consistent with the higher coulombic efficiency.

The voltage profile for cycle one, ten and forty for both flow field designs are shown in Figure 3 (c) and (d). The voltage profile during charge/discharge cycling of this system was stable and capacity fading was not observed during 40 cycles of operation at 20 mA cm^{-2} with a fixed charging time of 20,000 s, corresponding to a state-of-charge of 27.5%.

Although no previous studies of the FBT mode have been identified in the peer reviewed literature, a family of patent applications[44–47] have reported that use flow arrangement on the halogen side of zinc-halogen flow batteries, indicating that the approach can enhance the performance. In the current study, FBT was used on both the zinc and iodide side of the battery. The enhancement in battery performance observed with FBT mode on the zinc side alone (i.e. with FB mode on the iodine side), was greater than that observed with FBT mode on the iodine side alone (see Figure S4). It is thus clear that FBT mode enhances the performance of both electrodes in the zinc-iodide battery. Having all the flow going through electrodes (i.e. flow-through operation) on both sides of the battery (or on the zinc side alone) causes high pressure drop and resulted in capacity fade and limited cyclability. A comparison of using flow-through with FBT mode on both sides of the cell is shown in SI Figure S5.[48] In this study, the pressure drop and associated pumping loss of the FBT design was not investigated in detail. Further work will be needed to study the pressure drop in the FBT design since pumping loss is an important consideration for flow batteries. However, the additional flow path through the electrode in the FBT mode will ensure that the pressure drop is lower than that for the FB design. Furthermore, the changes in the zinc deposit morphology will also likely lead to a lower pressure drop for the FBT design. Raman spectroscopy analysis of the catholyte after the first and 40th cycles of charge/discharge is shown in the SI, (Figure S6). The Raman analysis indicates that no residual of I_3^- was evident in the fully discharged catholyte. The Raman results along with the observed coulombic efficiency shows a high system reversibility. The Raman spectra of the catholyte is consistent with previous studies.[7,49] Charge/discharge cycling was also performed at a lower current density of 10 mA cm^{-2} (see Figure S7). The energy efficiency

was around 90% throughout 40 cycles, and there was negligible capacity decay. Comparing the efficiency and cyclability obtained in this study to other studies of the zinc-iodide flow battery, the performance with the FBT operating mode has the highest reported efficiency and cyclability (see Table S1 in SI). For example Li et al. have reported an energy efficiency of 76% for a zinc-iodide RFB operating at a current density of 20 mA cm^{-2},[7] with slightly higher electrolyte concentration of 3.5 M ZnI_2. In this study, significantly higher energy efficiency of 84% at the same current density with a concentration of 3 M ZnI_2 (Table 1.) is reported. The energy density of the system was also compared with other studies.[7,42,50] The energy density reported by Li et al. was 125 Wh L^{-1}.[7] The energy density for the charge/discharge studies shown in Figure 3 were relatively low with values of 30.4 Wh L^{-1} and 27.6 Wh L^{-1} for FBT and FB modes respectively. However, considering the state-of-charge used of only 27.5%, the energy density is comparable with that reported by Li et al. At 100% state-of-charge, the obtained energy density in this study is 112 Wh L^{-1}, the specific capacity of the zinc-iodide battery in this study at a current density of 20 mA cm^{-2} and 40 mA cm^{-2} are shown in Figure S8. Areal capacity is an important parameter for deposition-based redox flow batteries.[51] At 100% state-of-charge and a current density of 20 mA cm^{-2}, an areal capacity of ca. 400 mAh cm^{-2} was achieved with the both the FBT and FB designs with electrolyte volumes of 20 ml on each side of the battery. However, further work is needed to determine the maximum areal capacity that can be achieved with these designs using larger volumes of electrolyte. Since more zinc is deposited within the depth of the felt electrode in the FBT mode, it is expected that a higher areal capacity could be achieved with this flow field design.

Effect of flow mode on the morphology of the zinc deposition

The morphology of the zinc deposit was evaluated by SEM and optical profilometry. Figure 4 shows SEM micrographs of the zinc electrode, after the 40^{th} charging cycle at a current density of 20 mA cm^{-2} (i.e. after the cycling shown in Figure 3). The micrograph of the zinc

deposit in the FB design is shown in Figure 4 (a). The micrograph depicts a fibrous growth with a rough anisotropic surface indicating higher overpotential during the zinc deposition during the charging process.[17] In the FBT design, a layer-like and compact zinc deposit was observed at the electrode surface, as shown in Figure 4 (b). The SEM micrographs of the electrode cross section, along with an EDS line-scan analysis through the depth of the electrode (Figure S9), illustrate the morphology and distribution of the zinc deposit on the surface and inside the electrode. A layer of zinc was deposited on the surface of the electrode close to the membrane (as indicated by white arrows in Figure S9), where the local current density is higher based on the porous electrode theory developed by Newman.[52,53] The EDS line scan shows that with the FBT design the zinc deposit penetrated further into the felt electrode, while for the FB design the deposit was confined to a dense layer at the surface close to the membrane. Zinc deposition was not observed on the graphite felt at the current collector side (as indicated by purple arrows in Figure S9). Deposition of zinc inside the felt provides evidence of enhanced mass transport in the FBT mode. In FB mode, there was no evidence of zinc deposition within the felt, suggesting that the fluid inside the pores was largely stagnant and deposition was severely limited by mass / ion transport. In contrast in FBT mode, the component of flow in the direction of the current feeder led to removal of stagnant fluid in the pores, and zinc deposition within the felt. Modifying the flow field from FB to FBT increased the convection mass transfer resulting in a thinner, smoother, and more compact zinc deposition. Since the deposit is more compact, with more zinc deposited inside the porous electrode in FBT mode, a higher zinc loading (and hence battery capacity) can be expected before the zinc deposit fills the flow channels. The increased zinc deposit inside the felt in FBT mode can be attributed to a higher rate of mass transfer inside the electrode in the FBT mode.

The optical profilometry 3D images of the surface of the zinc-coated electrodes after 40 cycles of charge/discharge are shown in Figure 5. Profilometry scan length was 800 μ m. and the scan was taken at the center of the electrode over an area of 16 mm × 14 mm.

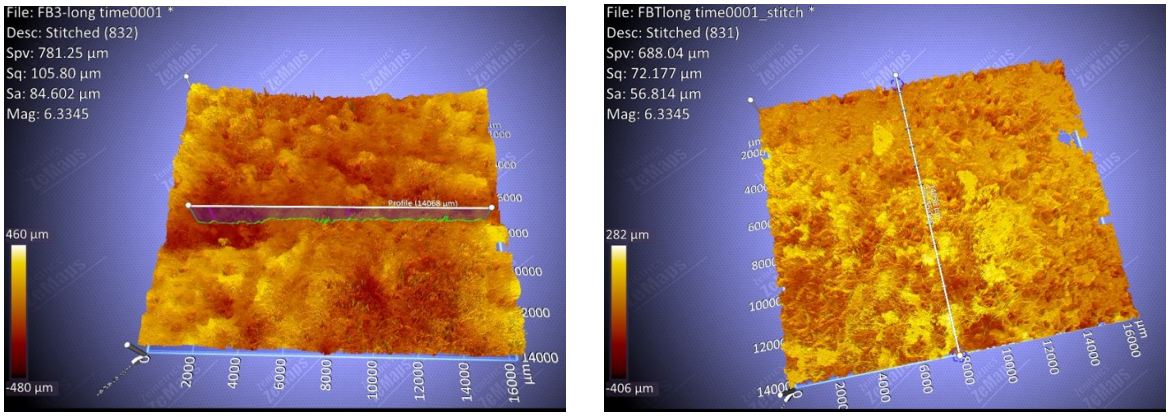

(a) (b)

Figure 5: Non contact-mode surface profilometry measurements of zinc deposition formed galvanostatically over 40 cycles at a current density of 20 mA cm^{-2}, and the solution is 3 M ZnI_2 in **(a)** FB design, and **(b)** FBT design.

The surface profilometry indicated that a rougher surface deposit for Zn-I RFB operated in the FB mode as compared to the FBT mode. The surface roughness S_a (the mean deviation of the surface height from the mean height) of the electrode surface was 84.6 µm and 56.4 µm for the FB and FBT modes respectively. The much smoother zinc deposit morphology observed in the zinc-iodide flow battery should enable a more stable operation at higher current densities using the FBT flow arrangement.

Based on the images obtained from SEM and OP, roughness and anisotropy of the zinc deposition in FB design leads to uneven zinc deposition and dendrite formation, but a smooth and compact deposit was observed with the FBT design, as well as some zinc deposition within the pores of the felt. This, combined with the higher charge efficiency, confirms that the FBT cell design mitigates dendrite formation at high state-of-charge and enhances the capacity and performance of the battery.

X-ray CT analysis

The use of X-ray CT to study electrode materials can provide new insights into processes occurring during battery cycling.[54] With X-ray CT, the thickness and quantity of zinc deposited inside the felt was analyzed. Figure 6 (a) and (b) show image analysis of the

carbon and zinc inside the felt under the compact zinc layer. Volume rendering of the graphite felt and zinc deposition inside the felt with two different flow modes were shown, and 2D slices of the data are shown in Figures S10 and S11. Around ten times more zinc was observed inside the porous felt in FBT electrode, as shown in the Table 2. X-ray CT images of the zinc deposit in the felt cross-section are shown in Figure 6 (c) and (d). The white region in these images illustrates the zinc layer deposited onto felt. The images show that most of the zinc was deposited as a layer within the felt, on the side of the felt close to the membrane. The thickness of the zinc layer in the felt was around 380 μm for FB and 280 μm for FBT operation, respectively. The zinc layer deposited on the felt in the FBT appears to be thinner and more compact compared with that observed in the FB mode. It was not possible to image the detailed structure of the zinc layer due to the high attenuation of the signal by the zinc metal. The noise in the 4 X images was caused by high attenuation of zinc which absorbs a large part of the X-ray beam. The total percentage of zinc inside the felt at 35% state-of-charge was 0.39% in the FB design and 2.5% in the FBT design. These results indicate that with the addition of some flow through the current feeder in FBT mode, the zinc inside the felt was replenished. This enhanced the mass transport and enabling the efficient deposition of a compact zinc layer on the felt surface.

Table 2: **Quantification of Zinc Deposition Inside the Felt monitored by X-ray CT**

Component	**Volume percentage-FB arrangement**[a]	**Percentage of solids**	**Volume percentage-FBT arrangement**[b]	**Percentage of solids**
Carbon	7.030	98.92	4.03	89.74
Zinc	0.076	1.08	0.47	10.26
Pore	92.89	-	95.5	-
Total	100	100	100	100.00

[a] FB: flow-by, [b] FBT: flow-by-through;

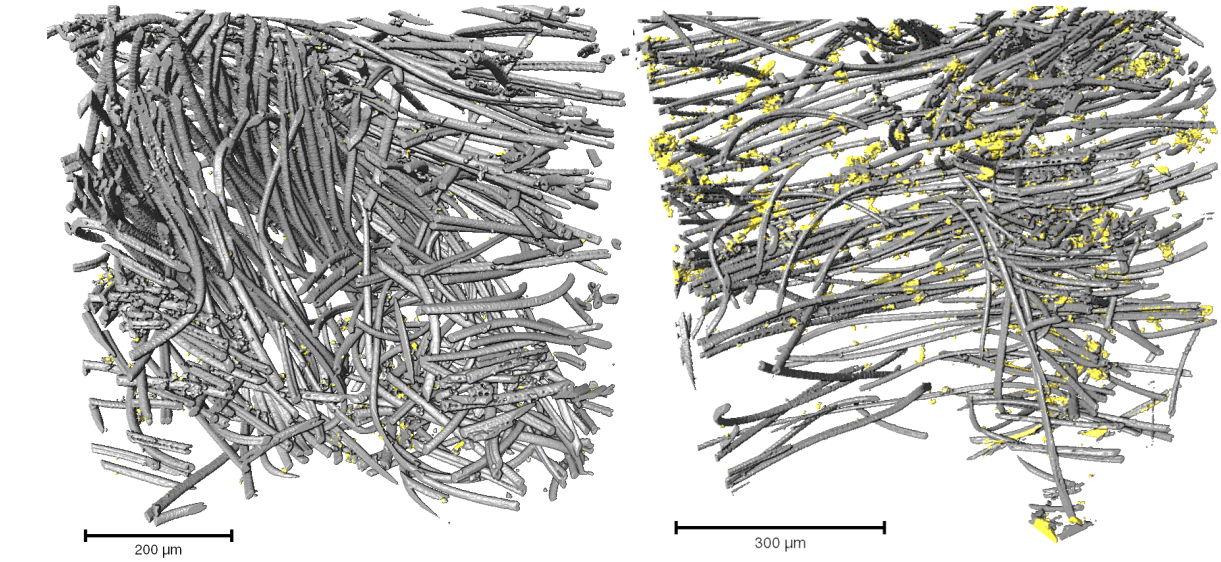

(a) (b)

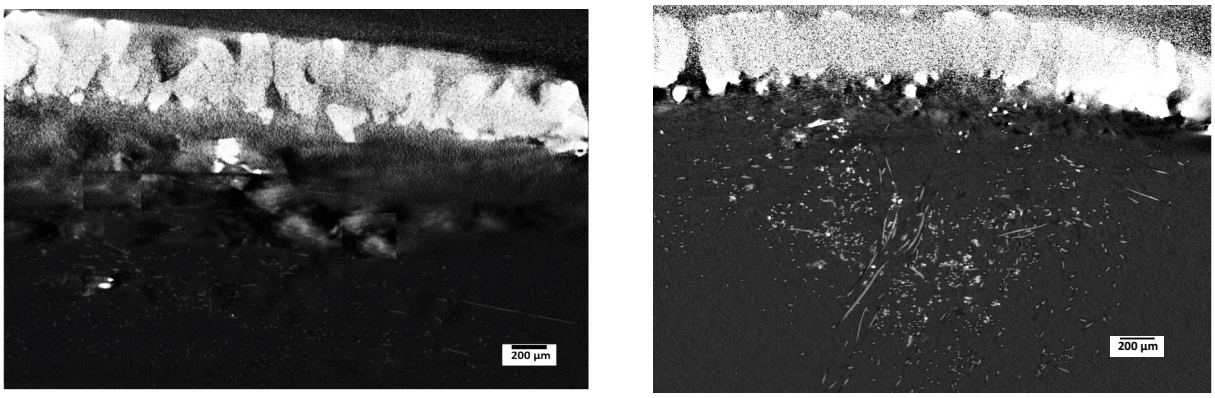

(c) (d)

Figure 6: Ex-situ X-ray micro tomography of zinc particles inside the felt, Volume rendering of the graphite felt and zinc deposition inside the felt in the **(a)** FB design, and **(b)** FBT design from the 20 X scans. Zinc layer deposition on the felt surface monitored by ex-situ X-ray tomography, **(c)** FB arrangement **(d)** FBT arrangement from 4 X scans. The corresponding state-of-charge for both test is 35%.

Conclusion

In this paper, the application of a novel flow field design on the performance of zinc-iodide batteries is presented. When compared to a conventional FB mode, significantly higher charge (99% vs. 96%) and energy (85% vs. 69%) efficiencies were obtained with a FBT arrangement. In the new flow design, having part of the flow go through the porous electrode enhanced the effective surface area and decreased the ohmic loss. The FBT design, with a component of flow in the direction of the current feeder, can prevent the blockage of the mass / ion transport pathway and enhance the flow distribution in hybrid flow batteries.[36] SEM, optical profilometry and X-ray CT were conducted to investigate the influence of the flow mode on the zinc deposit morphology. The FBT mode led to a more compact, smoother zinc deposition on the negative electrode and eliminated dendrite's growth at a current density of 20 mA cm^{-2}. Based on the X-ray CT and SEM characterization, with the FBT mode a denser zinc layer, and more zinc deposition inside the felt were observed, which may explain the increased discharge capacity and cycle life of the battery. In addition, in the FBT operating mode, reduced potential loss and overpotential were observed compared with FB operation. While the high energy density of the zinc-iodide RFB has been demonstrated, the current density (and hence power density) are limited during charging due to dendrite growth limiting cycling. This constraint will limit the application of this technology for mobile and transport applications, as a large battery size will be required. A Zn-based RFB using FBT design can achieve a higher current density and suppress zinc dendrite formation in comparison to conventional flow field designs. Dendrite formation is likely mitigated by the enhanced mass transport, which could enable operation at higher current densities without the operational problems that can occur with conventional FB designs.

The maximum discharge power density of 118 mW cm^{-2} obtained with this new flow field design is amongst the highest reported for a flow battery using ZnI_2 electrolyte.[42,43]

Acknowledgement

This document is the results of research project funded by the Natural Science and Engineering Research Council of Canada (NSERC CREATE 495455-2017 and RGPIN-2018-03725), and STFC batteries network. Financial support is highly appreciated.

Author Contribution

Fatemeh ShakeriHosseinabad: Conceptualization of the study, methodology, experimental work and analysis, sample preparation, preparation of the original manuscript draft. **Sohrab R. Daemi:** X-ray CT Characterization, editing and reviewing the manuscript **Damilola Y. Momodu:** Reviewing of the data and analysis, Raman characterization, ediring and reviewing the manuscript. **Paul R. Shearing and Dan J.L.Brett:** Supervision of X-ray CT Characterization, editing and reviewing the manuscript. **Edward P.L.Roberts:** Securing funding, supervision of the project, conceptualization of the study, methodology, editing and reviewing of the manuscript.

Supporting Information Available

The following files are available free of charge.

- Battery test cell and cross-sectional design
- Voltage profile for different flow field designs for each side of the battery
- Raman spectra analysis
- Cross sectional SEM images
- Voltage profile for the maximum energy density
- 2D virtual X-ray CT slices for two different flow field designs

References

(1) Leung, P.; Li, X.; De León, C. P.; Berlouis, L.; Low, C. J.; Walsh, F. C. Progress in redox flow batteries, remaining challenges and their applications in energy storage. *Rsc Advances* **2012**, *2*, 10125–10156.

(2) Li, X.; de León, C. P.; Walsh, F.; Wills, R. G.; Pletcher, D. *Advances in Batteries for Medium and Large-Scale Energy Storage*; Elsevier, 2015; pp 293–315.

(3) Weber, A. Z.; Mench, M. M.; Meyers, J. P.; Ross, P. N.; Gostick, J. T.; Liu, Q. Redox flow batteries: a review. *Journal of Applied Electrochemistry* **2011**, *41*, 1137.

(4) Soloveichik, G. L. Flow batteries: current status and trends. *Chemical reviews* **2015**, *115*, 11533–11558.

(5) Khor, A.; Leung, P.; Mohamed, M.; Flox, C.; Xu, Q.; An, L.; Wills, R.; Morante, J.; Shah, A. Review of zinc-based hybrid flow batteries: From fundamentals to applications. *Materials Today Energy* **2018**, *8*, 80–108.

(6) Xiong, B.; Zhao, J.; Tseng, K. J.; Skyllas-Kazacos, M.; Lim, T. M.; Zhang, Y. Thermal hydraulic behavior and efficiency analysis of an all-vanadium redox flow battery. *Journal of Power Sources* **2013**, *242*, 314–324.

(7) Li, B.; Nie, Z.; Vijayakumar, M.; Li, G.; Liu, J.; Sprenkle, V.; Wang, W. Ambipolar zinc-polyiodide electrolyte for a high-energy density aqueous redox flow battery. *Nature communications* **2015**, *6*, ncomms7303.

(8) Gong, K.; Ma, X.; Conforti, K. M.; Kuttler, K. J.; Grunewald, J. B.; Yeager, K. L.; Bazant, M. Z.; Gu, S.; Yan, Y. A zinc-iron redox-flow battery under $100 per kW h of system capital cost. *Energy & Environmental Science* **2015**, *8*, 2941–2945.

(9) Palomares, V.; Serras, P.; Villaluenga, I.; Hueso, K. B.; Carretero-González, J.; Rojo, T.

Na-ion batteries, recent advances and present challenges to become low cost energy storage systems. *Energy & Environmental Science* **2012**, *5*, 5884–5901.

(10) Higashi, S.; Lee, S. W.; Lee, J. S.; Takechi, K.; Cui, Y. Avoiding short circuits from zinc metal dendrites in anode by backside-plating configuration. *Nature communications* **2016**, *7*, 1–6.

(11) Lu, W.; Xie, C.; Zhang, H.; Li, X. Inhibition of Zinc Dendrite Growth in Zinc-Based Batteries. *ChemSusChem* **2018**, *11*, 3996–4006.

(12) Lee, B.-S.; Cui, S.; Xing, X.; Liu, H.; Yue, X.; Petrova, V.; Lim, H.-D.; Chen, R.; Liu, P. Dendrite suppression membranes for rechargeable zinc batteries. *ACS applied materials & interfaces* **2018**, *10*, 38928–38935.

(13) Iacovangelo, C. D.; Will, F. G. Parametric study of zinc deposition on porous carbon in a flowing electrolyte cell. *Journal of The Electrochemical Society* **1985**, *132*, 851.

(14) Fu, J.; Cano, Z. P.; Park, M. G.; Yu, A.; Fowler, M.; Chen, Z. Electrically rechargeable zinc–air batteries: progress, challenges, and perspectives. *Advanced materials* **2017**, *29*, 1604685.

(15) Vitos, L.; Ruban, A.; Skriver, H. L.; Kollár, J. The surface energy of metals. *Surface science* **1998**, *411*, 186–202.

(16) Wang, L.; Hoyt, J. J.; Wang, N.; Provatas, N.; Sinclair, C. W. Controlling solid-liquid interfacial energy anisotropy through the isotropic liquid. *Nature communications* **2020**, *11*, 1–7.

(17) Zhang, Q.; Amooie, A.; Bazant, M. Z.; Bischofberger, I. Growth morphology and symmetry selection of interfacial instabilities in anisotropic environments. *Soft Matter* **2021**, *17*, 1202–1209.

(18) Ben-Jacob, E.; Godbey, R.; Goldenfeld, N. D.; Koplik, J.; Levine, H.; Mueller, T.; Sander, L. Experimental demonstration of the role of anisotropy in interfacial pattern formation. *Physical review letters* **1985**, *55*, 1315.

(19) Wang, K.; Pei, P.; Ma, Z.; Chen, H.; Xu, H.; Chen, D.; Wang, X. Dendrite growth in the recharging process of zinc–air batteries. *Journal of Materials Chemistry A* **2015**, *3*, 22648–22655.

(20) Huang, S.; Li, H.; Pei, P.; Wang, K.; Xiao, Y.; Zhang, C.; Chen, C. A dendrite-resistant zinc–air battery. *Iscience* **2020**, 101169.

(21) Yufit, V.; Tariq, F.; Eastwood, D. S.; Biton, M.; Wu, B.; Lee, P. D.; Brandon, N. P. Operando visualization and multi-scale tomography studies of dendrite formation and dissolution in zinc batteries. *Joule* **2019**, *3*, 485–502.

(22) Lamping, B. A.; O'Keefe, T. J. Evaluation of zinc sulfate electrolytes by cyclic voltammetry and electron microscopy. *Metallurgical Transactions B* **1976**, *7*, 551–558.

(23) Diggle, J.; Despic, A.; Bockris, J. The mechanism of the dendritic electrocrystallization of zinc. *Journal of The Electrochemical Society* **1969**, *116*, 1503–1514.

(24) Cheng, X.-B.; Zhang, R.; Zhao, C.-Z.; Zhang, Q. Toward safe lithium metal anode in rechargeable batteries: a review. *Chemical reviews* **2017**, *117*, 10403–10473.

(25) Zhang, K.; Yan, Z.; Chen, J. Electrodeposition Accelerates Metal-Based Batteries. *Joule* **2020**, *4*, 10–11.

(26) Wang, R.; Kirk, D.; Zhang, G. Effects of deposition conditions on the morphology of zinc deposits from alkaline zincate solutions. *Journal of The Electrochemical Society* **2006**, *153*, C357–C364.

(27) Naybour, R. Morphologies of zinc electrodeposited from zinc-saturated aqueous alkaline solution. *Electrochimica Acta* **1968**, *13*, 763–769.

(28) Bockris, J.; Nagy, Z.; Drazic, D. On the morphology of zinc electrodeposition from alkaline solutions. *Journal of The Electrochemical Society* **1973**, *120*, 30.

(29) Gavrilović-Wohlmuther, A.; Laskos, A.; Zelger, C.; Gollas, B.; Whitehead, A. H. Effects of electrolyte concentration, temperature, flow velocity and current density on Zn deposit morphology. *J. Energy Power Eng* **2015**, *9*, 1019–1028.

(30) Naybour, R. The effect of electrolyte flow on the morphology of zinc electrodeposited from aqueous alkaline solution containing zincate ions. *Journal of The Electrochemical Society* **1969**, *116*, 520–524.

(31) Chen, C.-P. Effect of Impinging Flow on the Morphology for Zinc Deposits. *Journal of The Electrochemical Society* **1990**, *137*, 212C–215C.

(32) Moshtev, R.; Zlatilova, P. Kinetics of growth of zinc dendrite precursors in zincate solutions. *Journal of Applied Electrochemistry* **1978**, *8*, 213–222.

(33) Liu, H.; Li, P.; Juarez-Robles, D.; Wang, K.; Hernandez-Guerrero, A. Experimental study and comparison of various designs of gas flow fields to PEM fuel cells and cell stack performance. *Frontiers in Energy Research* **2014**, *2*, 2.

(34) Ito, Y.; Wei, X.; Desai, D.; Steingart, D.; Banerjee, S. An indicator of zinc morphology transition in flowing alkaline electrolyte. *Journal of Power Sources* **2012**, *211*, 119–128.

(35) Svensson, P. H.; Kloo, L. Synthesis, structure, and bonding in polyiodide and metal iodide- iodine systems. *Chemical reviews* **2003**, *103*, 1649–1684.

(36) Zhou, X.; Lin, L.; Lv, Y.; Zhang, X.; Fan, L.; Wu, Q. Elucidating effects of component materials and flow fields on Sn–Fe hybrid flow battery performance. *Journal of Power Sources* **2020**, *450*, 227613.

(37) Zhou, X.; Lin, L.; Lv, Y.; Zhang, X.; Wu, Q. A Sn-Fe flow battery with excellent rate and cycle performance. *Journal of Power Sources* **2018**, *404*, 89–95.

(38) Leung, P.; Ponce-de Leon, C.; Low, C.; Shah, A.; Walsh, F. Characterization of a zinc–cerium flow battery. *Journal of Power Sources* **2011**, *196*, 5174–5185.

(39) Feldkamp, L. A.; Davis, L. C.; Kress, J. W. Practical cone-beam algorithm. *Josa a* **1984**, *1*, 612–619.

(40) Yin, Y.; Wang, S.; Zhang, Q.; Song, Y.; Chang, N.; Pan, Y.; Zhang, H.; Li, X. Dendrite-free zinc deposition induced by tin-modified multifunctional 3D host for stable zinc-based flow battery. *Advanced Materials* **2020**, *32*, 1906803.

(41) Trudgeon, D. P.; Qiu, K.; Li, X.; Mallick, T.; Taiwo, O. O.; Chakrabarti, B.; Yufit, V.; Brandon, N. P.; Crevillen-Garcia, D.; Shah, A. Screening of effective electrolyte additives for zinc-based redox flow battery systems. *Journal of Power Sources* **2019**, *412*, 44–54.

(42) Weng, G.-M.; Li, Z.; Cong, G.; Zhou, Y.; Lu, Y.-C. Unlocking the capacity of iodide for high-energy-density zinc/polyiodide and lithium/polyiodide redox flow batteries. *Energy & Environmental Science* **2017**, *10*, 735–741.

(43) Jian, Q.; Wu, M.; Jiang, H.; Lin, Y.; Zhao, T. A trifunctional electrolyte for high-performance zinc-iodine flow batteries. *Journal of Power Sources* **2021**, *484*, 229238.

(44) Cole, R.; Winter, R.; Hall, J.; Pharkya, P.; Hart, J. l. O., Gerardo; Lauren, W.; Kreiner, P.; Tennessen, P. Fluidic architecture for metal-halogen flow battery. 2015; US Patent 9,130,217.

(45) Winter, R.; Hall, J. L.; Pharkya, P.; Kreiner, P.; Cole, R.; Gerardo, J. l. O. Electrolyte flow configuration for a metal-halogen flow battery. 2016; US Patent 9,478,803.

(46) Haynes, K.; Kreiner, P.; Hall, J. L.; Kell, B.; Winter, R. Metal Electrode Assembly for Flow Batteries. 2012; US Patent App. 13/470,918.

(47) Winter, R. O. Electrochemical energy cell system. 2009; US Patent App. 11/654,380.

(48) Zeng, Y.; Li, F.; Lu, F.; Zhou, X.; Yuan, Y.; Cao, X.; Xiang, B. A hierarchical interdigitated flow field design for scale-up of high-performance redox flow batteries. *Applied energy* **2019**, *238*, 435–441.

(49) Wakita, H.; Johansson, G.; Sandström, M.; Goggin, P. L.; Ohtaki, H. Structure determination of zinc iodide complexes formed in aqueous solution. *Journal of solution chemistry* **1991**, *20*, 643–668.

(50) Zhang, J.; Jiang, G.; Xu, P.; Kashkooli, A. G.; Mousavi, M.; Yu, A.; Chen, Z. An all-aqueous redox flow battery with unprecedented energy density. *Energy & Environmental Science* **2018**, *11*, 2010–2015.

(51) Yao, Y.; Lei, J.; Shi, Y.; Ai, F.; Lu, Y.-C. Assessment methods and performance metrics for redox flow batteries. *Nature Energy* **2021**, *6*, 582–588.

(52) Newman, J.; Tiedemann, W. Porous-electrode theory with battery applications. *AIChE Journal* **1975**, *21*, 25–41.

(53) Hawthorne, K. L.; Wainright, J. S.; Savinell, R. F. Maximizing plating density and efficiency for a negative deposition reaction in a flow battery. *Journal of Power Sources* **2014**, *269*, 216–224.

(54) Schröder, D.; Bender, C.; Arlt, T.; Osenberg, M.; Hilger, A.; Risse, S.; Ballauff, M.; Manke, I.; Janek, J. In operando x-ray tomography for next-generation batteries: a systematic approach to monitor reaction product distribution and transport processes. *Journal of Physics D: Applied Physics* **2016**, *49*, 404001.

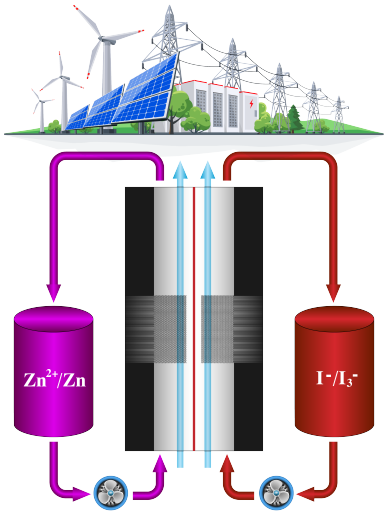

Conventional flow-by

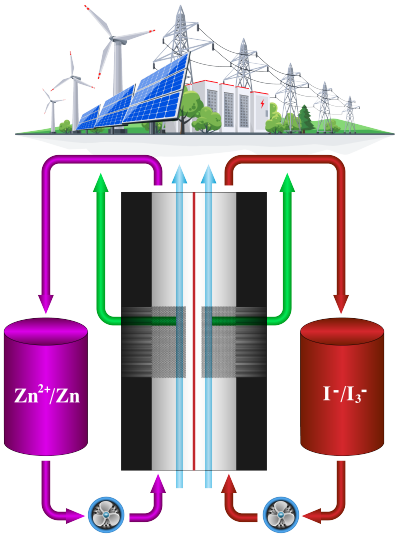

Novel: Flow-by-through

Rough and porous zinc deposition

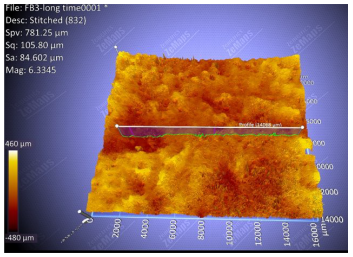

Energy Efficiency
64% at 30 mA cm^{-2}
Max. power density
104 mW cm^{-2}

Compact-soft zinc deposition

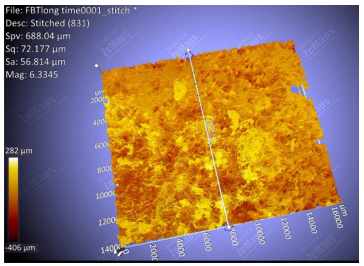

Energy Efficiency
74% at 30 mA cm^{-2}
Max. power density
118 mW cm^{-2}

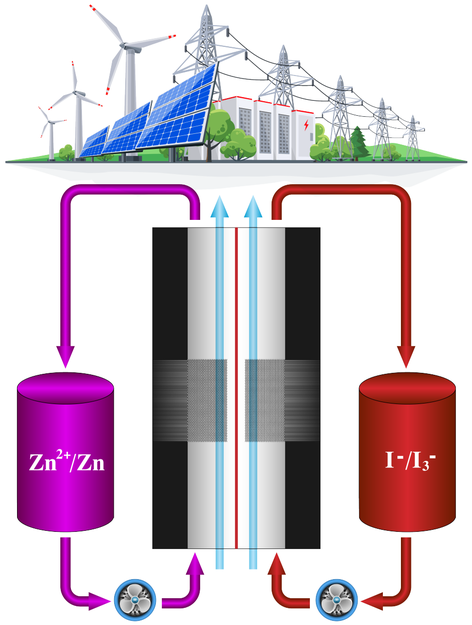

Conventional flow-by

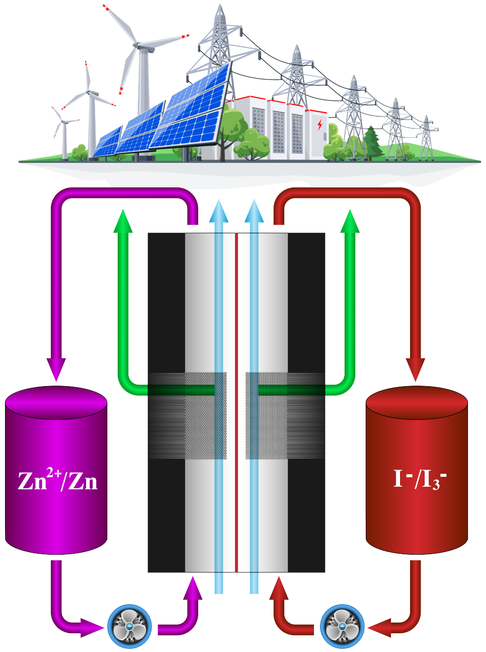

Novel: Flow-by-through

Rough and porous zinc deposition

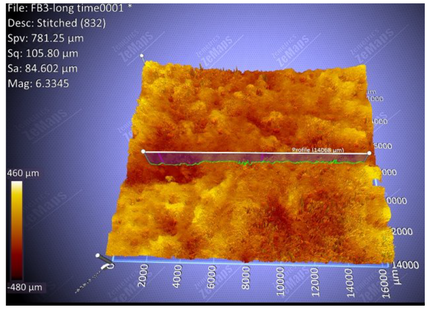

Energy Efficiency
64% at 30 mA cm^{-2}
Max. power density
104 mW cm^{-2}

Compact-soft zinc deposition

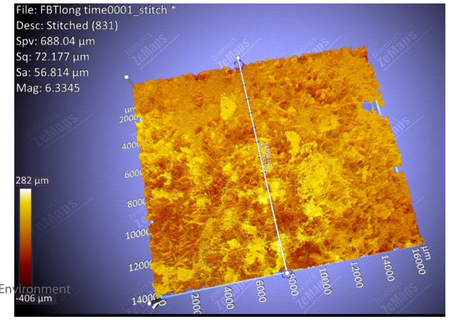

Energy Efficiency
74% at 30 mA cm^{-2}
Max. power density
118 mW cm^{-2}